

Genesis and geological significance of carbonate in Changdu Basin, Xizang, China: Constraints from geochemistry and C–O isotopes

Wenhua Han^{1,2} · Yongshou Li^{1,2} · Haizhou Ma^{1,2} · Huaide Cheng^{1,2} · Binkai Li^{1,2} · Qinyu Hai^{1,2} · Xuahai Ma^{1,2}

Received: 20 November 2023 / Revised: 11 April 2024 / Accepted: 16 May 2024 / Published online: 27 May 2024

© The Author(s), under exclusive licence to Science Press and Institute of Geochemistry, CAS and Springer-Verlag GmbH Germany, part of Springer Nature 2024

Abstract Research on the origin of carbonates in Changdu Basin holds significant importance for understanding the regional potash formation model. Based on a comprehensive review of previous studies, field geological surveys, and laboratory investigations, this study analyzes the origin and properties of carbonates within the context of regional potash formation. Petrographic studies show that magnesite deposits, with the characteristics of sedimentary origin. The results of elemental geochemical analysis show that the carbonates in this area were formed in the sedimentary environment via evaporation followed by concentration, and the formation of magnesite was possibly caused by the substitution of calcium in the dolomite with magnesium-rich brine. The $\delta^{13}\text{C}$ values of carbonates in the study area are between 5.9‰ and 9.1‰. The $\delta^{18}\text{O}$ values of magnesite samples range from –7.3‰ to –1.3‰, and the $\delta^{18}\text{O}$ values of dolomites range from –10.3‰ to –8.4‰. All the calculated Z values of oxygen isotopes of carbonates greater than 120. A comprehensive analysis of carbon and oxygen isotopes indicates that the magnesite was formed in a highly concentrated Marine sedimentary environment and does not show any relation with the metasomatism of hydrothermal fluids. The results on the correlation of magnesite with seawater and its sedimentary origin provide key information for explaining the migration direction of brine between the Changdu and Lanping–Simao Basins. The residual metamorphic seawater in the Changdu Basin migrated to the Lanping–Simao Basin,

where potash underwent deposition. Whereas, magnesite and dolomite in the early stage of potash formation were left in the Changdu Basin.

Keywords Changdu basin · Carbonatite · Geochemistry · Mineral deposit genesis · Significance of potash formation

1 Introduction

The Changdu Basin is located in the eastern part of the Tethys metallogenic belt, while its southern counterpart is the Lanping and Simao Basin, extending south into Laos, Thailand, and adjacent to the Korat Plateau. Together, these basins constitute a vast basin system (Su et al. 2007; Li et al. 2008; Pan et al. 2012; Wu et al. 2020). Recent studies have shown that seawater serves as a rich potash-forming source for the potash deposit in the Lanping–Simao and Korat Basins. Moreover, the Changdu–Lanping–Simao–Korat Basin functioned as a unified and interconnected large-scale evaporation basin during a transgression period (Wang et al. 2014a, b; Gao et al. 2013; Han et al. 2021). Some scholars have proposed that the extensive evaporites found in the Changdu–Lanping–Simao Basin resulted from the Tethys Ocean seawater entering the salt belt basins in the form of concentrated metamorphic seawater after passing through the north of the restricted Qiangtang Sea. This proposal suggests the involvement of a multi-stage basin seawater concentration model, metamorphism, and migration, leading to salt and potash formation. The Changdu Basin serves as a preparatory basin in the regional mineralization process (Li 2015; Han et al. 2021). Noteworthy, the establishment of this mineralization model primarily relies on the geological characteristics of salt-bearing basins and

✉ Yongshou Li
yongshouli@isl.ac.cn

¹ Key Laboratory of Comprehensive and Highly Efficient Utilization of Salt Lake Resources, Qinghai Institute of Salt Lakes, Chinese Academy of Sciences, Xining 810008, China

² Qinghai Provincial Key Laboratory of Geology and Environment of Salt Lakes, Xining 810008, China

seawater evaporation experiments (Li 2015). According to the normal seawater evaporation results and deposition theory, significant deposition of sulfate and carbonates should accompany potash deposition. However, substantial production of sulfate (gypsum) and carbonate rocks (magnesite) remains unobserved in the potash deposits of the Lanping–Simao Basin and the Khorat Basin (Li 2015). Experiments demonstrate that magnesite formation under typical seawater evaporation conditions is unattainable. When water containing HCO_3^- enters the seawater and the Mg/Ca ratio becomes abnormally high, then only magnesite can precipitate, which closely aligns with the potash precipitation stage (Li 2015).

Significant magnesite deposits exist in Baxia, Kamaduo Township, within the Changdu Basin. Some scholars have suggested that the origin of magnesite in the Changdu can be associated with ultramafic weathering leaching or metasomatism of magnesia-rich fluids (Ding et al. 2013). However, in-depth research on the deposit has rarely been carried out to date. Following several field geological surveys, this study indicates that the magnesite is stratified, with no apparent alteration, displaying uniform ore texture and a distinct boundary between the ore-bearing layer and dolomite. These field characteristics make the magnesite deposition and ultrabasic rock formation through weathering leaching and metasomatism of hydrothermal fluids, very unlikely. Consequently, given the extensive Marine gypsum exposure in the basin (Li 2015), combined with the characteristics of seawater evaporation experiments and regional evaporite deposits, it is hypothesized that the formation of this deposit is related to the replacement of dolomite with magnesium-rich seawater, rather than the direct replacement of ultramafic rocks via magnesium-rich hydrothermal mineralization. Comprehensive comparative analysis demonstrates that the sulfates (gypsum) and carbonates (Dolomite and magnesite) present at the early stage of potash formation in the Lanping–Simao Basin might have originated in the Changdu Basin. Subsequently, tectonic movements likely facilitated the migration of metamorphic seawater to these areas. However, within the geological context of exploring regional mineralization models, in-depth research on magnesite deposits in the Changdu Basin remains pending, significantly limiting the exploration of the mineralization of the above-mentioned models. Systematic exploration of the genesis of magnesite in the Changdu Basin is scientifically vital for indicating the migration pattern of metamorphic seawater. Therefore, this study focuses on the magnesite deposits in Baxia as a research object. This study relies on previous research results, combines detailed field geological surveys, employs petrographic and geochemical methods to explore the origin of the deposit, and further discusses

the regional salt and potash formation model within the Changdu–Lanping–Simao Basin.

2 Geological setting

Magnesite deposit is located in the Baxia, Kamaduo township, in the west of Changdu City ($31^{\circ}07'37''$ N, $96^{\circ}30'02''$ E) (Fig. 1). It is located within the Sanjiang fault belt and the Lancangjiang fold belt (Fig. 1B). Various tectonic events, including the Caledonian orogeny, Hercynian orogeny, Yanshanian movement, and others, caused a series of left-running, en echelon complex anticlines and extensive fault zones extending from the north to west. In the western part of the study area, ultramafic rocks related to the Indo-chine–Yanshanian tectonic movement are present, which represent the eastward extension of the Dingqing–Dongqiao ultramafic rock distribution belt. The orientation of the magnesite ore body aligns with the deep fault-controlled distribution of ultramafic rocks in the area. The ultramafic lithotypes in this region predominantly consist of serpentinite, peridotite, and pyroxenite. The magnesite ore body is mainly found at secondary fault locations and contact points with dolomite, showing gradual transitions with dolomite. At these contact points, angular dolomite clasts can be observed (Xie 2007).

In this study area, the primary exposed strata are represented by the Middle Jurassic Yanshiping Group (J_2ys) and the Lower Jurassic Luodong Group (J_2d) (Fig. 2A). The Yanshiping Group (J_2ys) is the primary ore-bearing formation that covers a significant portion of the mining area. It predominantly comprises purplish red sandstone with conglomerate, dolomite, limestone, and gray medium to coarse-grained feldspar quartz sandstone. The main ore-bearing layer, situated in the central part of the mining area, is primarily composed of a set of dolomitic limestones. The bottom layer beneath the magnesite layer is the Middle Jurassic Luodong Group (J_2d), which is in fault contact with the Yanshiping Group. The upper section of the magnesite ore body consists of dolomite, with the prevalent types being powdery dolomite and sandy dolomite, typically exhibiting gray-black coloration and massive structures (Fig. 2B). The magnesite ore body primarily occurs within dolomite of the Middle Jurassic Yanshiping Group. The contact layer between the ore body and the surrounding rock typically consists of brecciated magnesite, with a distinct boundary between dolomite and magnesite (Fig. 2C, D). The surrounding rock environment of magnesite mainly consists of dolomite, limestone, sandstone, and sandy conglomerate; and occasionally, silty mudstone and dolomitic mudstone can be observed. The surrounding rock possesses a medium hardness. The occurrence of the magnesite layer closely aligns with the surrounding rock dolomite, featuring a stratified structure (Fig. 2B, C).

Fig. 1 **A** Simplified geological map of the study area (modified after Xie 2007), 1. Yanshiping Group; 2. Luodong Group; 3. ultramafic rocks; 4. dolerite; 5. magnesite deposit; 6. fault; 7. highway; 8. study area; 9. suture zone; 10. river; 11. location. **B** Schematic tectonic map of Changdu Basin. KS: South Kunlun Suture Zone; JS: Jinshajiang Suture Zone; BNS: Bangong-Nujiang Suture Zone; and ITS: Indus-Tsangpo Suture Zone (modified after Qi 2017)

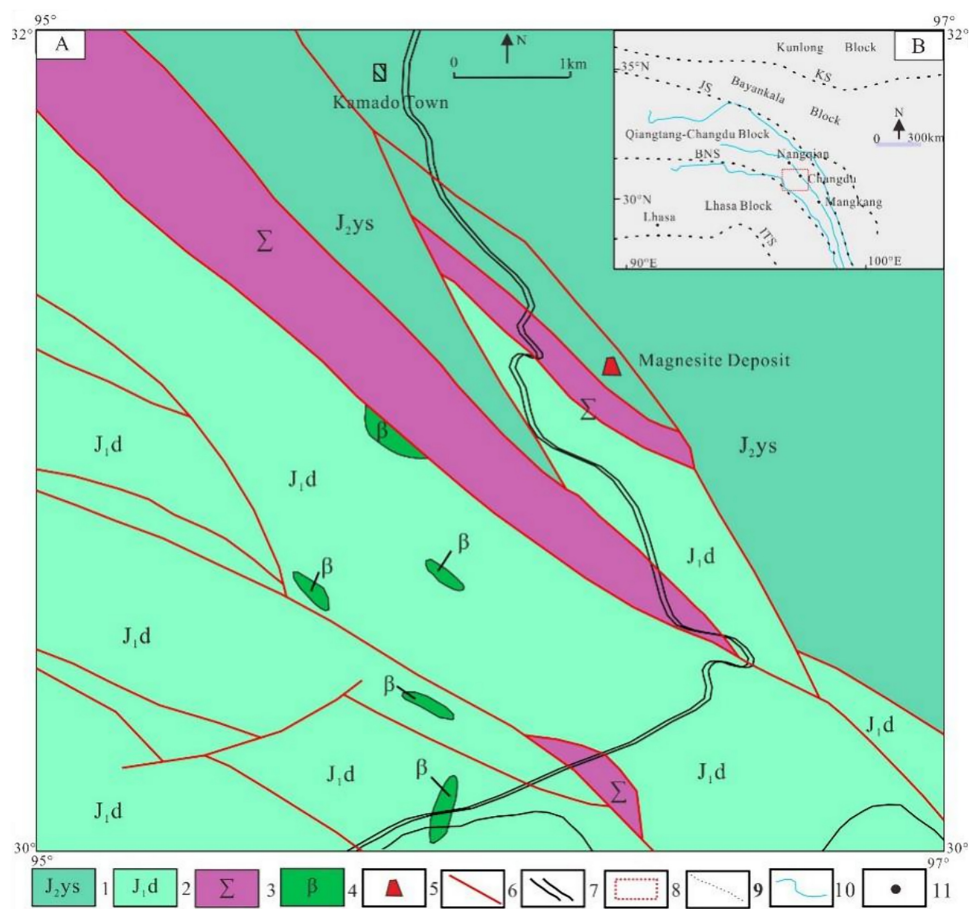
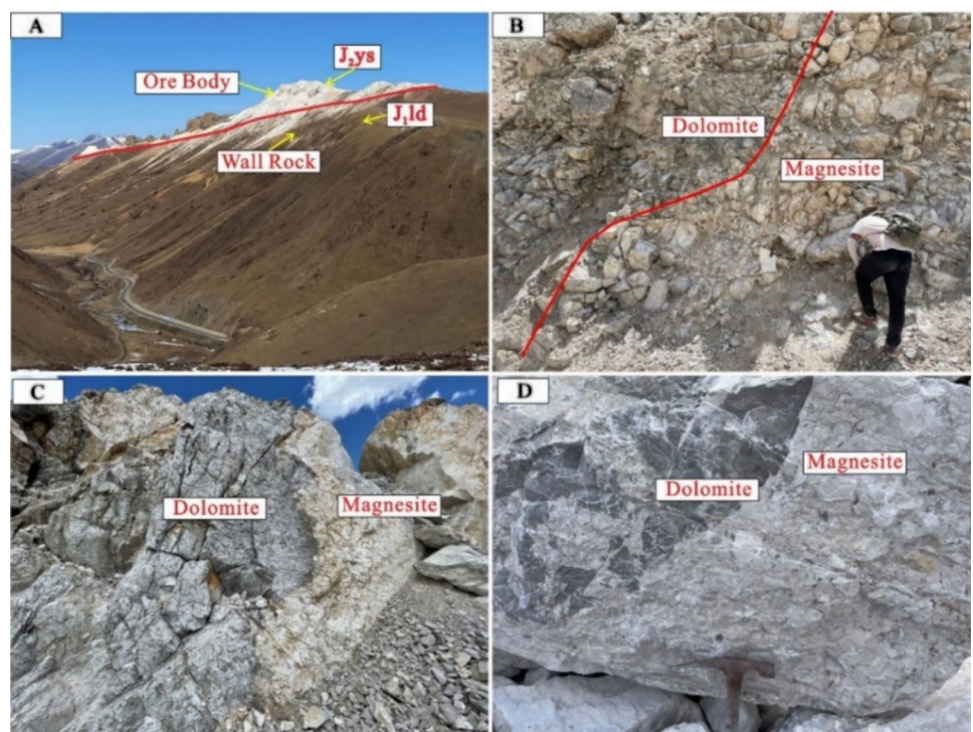


Fig. 2 Characteristics of the magnesite ore body: **A** field photograph of ore body; **B** contact between dolomite and magnesite; **C** the contact between the ore body and the wall rock; and **D** brecciate magnesite



The upper surrounding rock consists mainly of dolomite, while some ore bodies are surrounded by limestone, where the limestone dissolution process is significantly developed. Dolomite exhibits sandy, granular, powdery fine crystals and block structures. The dolomite roof above the magnesite ore body displays significant alteration, is primarily calcareous, and shows local chloritization and silicification. The surrounding rock on the floor consists of siltstone, sandstone, a minor amount of sandy conglomerate, and mudstone. This also indicates that the residual, thick layer-block structures are primarily composed of quartz sand. The predominant cement type in the surrounding rock is mainly siliceous, followed by calcareous.

3 Materials and methods

In this study, nine samples, comprising six magnesite samples and three dolomite samples, were collected from the surrounding rock. These samples underwent various analyses, including thin section petrography, whole rock X-ray diffraction (XRD), Inductively coupled plasma-mass spectroscopy (ICP-MS) elemental geochemistry, and carbon and oxygen isotope analysis. XRD analysis was conducted using a D8AA25 X-ray diffractometer with a focal spot size of 0.4×12 mm. Mineral scanning was carried out using a goniometer. This analysis was performed at the Qinghai Institute of Salt Lake Research, Chinese Academy of Sciences. Geochemical analysis of carbon and oxygen isotopes, as well as major and trace elements of the samples, was conducted in the laboratory of the Beijing Research Institute of Uranium Geology, Beijing, China. A major element of the samples was fused with a lithium metaborate–lithium tetraborate flux containing an oxidizing agent (lithium nitrate) and then poured into a platinum mold for analysis. Based on rock standards and duplicate sample analysis, analytical reproducibility was generally within 5% for significant oxides. Loss on ignition (LOI) was measured by heating the powdered sample (1 g) at 1100 °C for 1 h. Trace element concentrations were measured by ICP-MS (Finnigan MAT Element). About 100 mg of entire rock powder was digested by a mixture of concentrated HNO_3 and HCl in screw-top PTFE-lined stainless-steel bombs at 190 °C. Details regarding the Q-ICP-MS analysis were described previously by Liang et al. (2000). The analytical precision was generally better than 10% for all elements based on rock standards and duplicate sample analysis. Carbon and oxygen isotope compositions were measured using a Finnigan MAT 253 mass spectrometer coupled with a Thermo Finnigan Gas Bench II system. First, the carbonate sample was ground to 200 mesh in an agate mortar, and then it was baked in an oven at 105 °C for 2 h to remove adsorbed water. Next, the sample tube was baked in a Gas

Bench online sampling equipment at 70 °C for 30 min, and then the sample with a carbonate content of approximately 0.2 mg was placed in a sample tube and the tube was then sealed. High-purity helium was used to remove air from the sample tube. An excess of 100% phosphoric acid was added to the sample tube using an acid pump acid needle. Phosphoric acid was allowed to react with the carbonate sample for over 8 h to produce CO_2 gas. High-purity helium was employed to introduce the generated CO_2 gas into the MAT253 mass spectrometer for testing the C and O isotope composition. Standard GBW04416 and GBW04417 were added to every five samples and compared with reference gas for testing. The test results for carbon and oxygen isotopes were presented using V-PDB (Pee Dee Belemnite) as the relative standard, denoted as $\delta^{13}\text{CV-PDB}$ (accuracy better than 0.1‰) and $\delta^{18}\text{OV-PDB}$ (accuracy better than 0.2‰), respectively. First, a reference gas was utilized to preliminarily calibrate the sample and reference substance. Finally, GBW04416 and GBW04417 standards were employed for double standard calibration and providing the calibration values for the sample.

4 Results

4.1 Petrography

Macroscopically, the fresh surface of magnesite predominantly appears milky or white, occasionally exhibiting a flesh-red and earthy luster. Dense magnesite fractures display a shell-like, conchoidal appearance (Fig. 3A). The contact area between the ore body and the surrounding rock comprises micritic magnesite, dolomitic breccia, dolomite debris, and a limited quantity of siliceous rock, quartzose sandstone, and other clasts (Fig. 3B). Dolomite and other mineral fragments get cemented together by dolomite, magnesite, calcite, illite, kaolinite, limonite, and other minerals. Micritic magnesite breccia, dolomite breccia, and clasts are angular and subangular, with breccia grain sizes ranging from 2.0 to 25.0 mm and clastic grain sizes ranging from 0.02 to 2.0 mm. Some clasts fill irregular fissures, forming columnar magnesite structures with curved algal laminae with larger grain sizes, resulting in the formation of crust-like structures. The mineral composition primarily includes micritic magnesite and micritic dolomite, with a minor amount of clay minerals. Pyrite constitutes approximately 1% and occasionally appears as cube-shaped or pentagonal dodecahedral euhedral crystals. Within the fissures of micritic carbonate, lamellar carbonates line the fissure walls, with darker areas indicating higher argillaceous content and relatively pure recrystallized carbonate crystals occupying the middle of the fissures. Microscopically, magnesite exhibits a micrite structure, followed by an alloid granular

Fig. 3 Macro and micro images of the sample: **A** fresh magnesite; **B** magnesite breccia; **C** recrystallized carbonate; **D** crusty structure

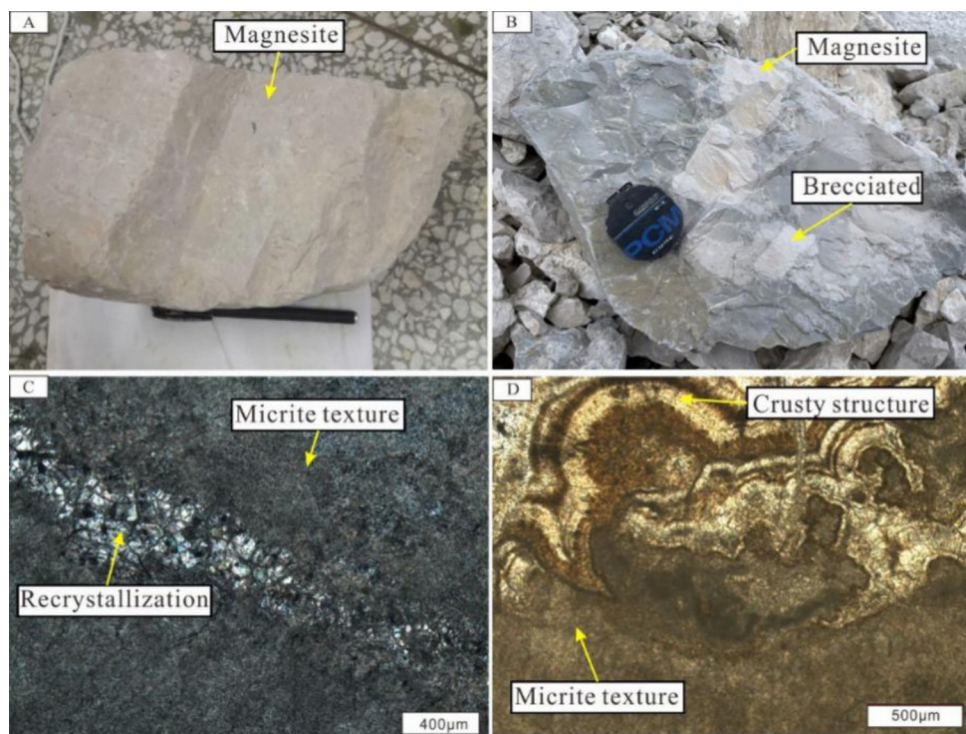


Table 1 XRD results

Sample	Magnesite (%)	Dolomite (%)	Quartz (%)	Lithology
BX-3	98	2	—	Magnesite
BX-4	98	1	—	Magnesite
BX-5A	63	37	1	Dolomite
BX-5B	95	5	—	Magnesite
BX-6	100	—	—	Magnesite
BX-8	66	25	10	Dolomite
BX-9	78	16	6	Dolomite
LMK-2	98	2	—	Magnesite
BX-12	97	2	—	Magnesite

structure and occurrence of intense recrystallization processes (Fig. 3C). In some localities, crusty structures surrounded by micritic dolomite grains can be observed (Fig. 3D). Magnesite primarily consists of micrite and aggregates, with particle sizes ranging from ~0.001 to 0.01 mm, mostly falling within the range of 0.003–0.006 mm. Only a small portion (5%–10%) of magnesite consists of granular particles with sizes between 0.01 and 0.4 mm, which fill irregular cracks.

In this study, semi-quantitative XRD analysis was conducted on samples from both the magnesite-bearing layer and the surrounding rock (Table 1). The results indicate that the ore-bearing layer is characterized by high-purity magnesite content. One sample consists of 100% magnesite with no accessory minerals, while others contain magnesite with a

minor percentage (2%–5%) of dolomite. In the surrounding rock dolomites, varying levels of quartz are present. The primary composition of dolomite reveals that magnesite content is notably higher than that of dolomite, with quartz content reaching up to 10%.

4.2 Geochemical characteristics

4.2.1 Major and trace elements

The results of the major and trace element analyses of magnesite and surrounding rock dolomite in the magnesite-bearing layer are listed in Table 2. The elemental analysis of the samples reveals the following characteristics:

For magnesite, the SiO₂ content is lower than 1%. The contents of Al₂O₃, Fe, Na₂O, K₂O, TiO₂, P₂O₅, and MnO are low. MgO and LOI are the dominant components, ranging from 45.97% to 47.89% and 50.82% to 51.36%, respectively. The CaO content ranges from 0.29% to 0.92%, except for one magnesite sample (BX-5B: 2.37%). The Sr concentrations range between 2.5 and 25.1 ppm, except for one magnesite sample (BX-4: 72.8 ppm). For the dolomite samples, the SiO₂ content ranges from 0.84% to 1.36%, except for one sample (BX-8: 7.20%), and the MgO contents range from 31.34% to 41.86%. Further, the CaO contents range from 5.93% to 7.08%, except for one sample (BX-5A: 18.73%). The Al₂O₃, Fe, Na₂O, K₂O, TiO₂, P₂O₅, and MnO contents are lower than 1%. The LOI ranges from 46.24% to 49.59%. The

Table 2 Major oxides (wt.%) and trace element (ppm) concentrations

Element	BX-3 Magnesite	BX-4 Magnesite	BX-5A Dolomite	BX-5B Magnesite	BX-6 Magnesite	BX-8 Dolomite	BX-9 Dolomite	LMK-2 Magnesite	BX-12 Magnesite
SiO ₂	0.34	0.18	0.84	0.33	0.22	7.20	1.36	0.29	0.37
Al ₂ O ₃	0.13	0.08	0.48	0.17	0.10	0.43	0.86	0.13	0.13
Fe	0.21	0.09	0.47	0.27	<0.01	0.70	0.21	0.05	<0.01
FeO	0.15	<0.10	0.40	0.20	<0.10	0.55	0.15	<0.10	<0.10
MgO	46.98	47.43	31.34	45.97	47.63	38.19	41.86	47.55	47.89
CaO	0.79	0.92	18.73	2.37	0.65	7.08	5.93	0.61	0.29
Na ₂ O	0.10	<0.01	0.05	<0.01	<0.01	<0.01	<0.01	<0.01	<0.01
K ₂ O	0.03	0.01	0.07	0.02	0.02	0.09	0.13	0.02	0.02
MnO	0.01	0.01	0.06	0.02	—	0.02	0.01	0.02	—
TiO ₂	<0.01	<0.01	0.03	<0.01	<0.01	0.02	0.03	<0.01	<0.01
P ₂ O ₅	0.01	0.01	0.01	0.01	0.01	0.02	0.02	0.01	0.01
LOI	51.36	51.25	47.84	50.82	51.33	46.24	49.59	51.30	51.28
Li	76.5	24.2	9.7	23.1	30.4	21.1	20.4	24.1	13.2
Be	0.18	0.05	0.44	0.36	0.05	0.26	0.16	0.21	0.01
Sc	0.34	0.07	1.49	0.16	0.14	0.99	1.21	0.12	0.12
V	6.36	2.82	8.56	4.24	1.58	7.54	9.15	1.5	0.55
Cr	167	113	54.5	10.4	5.02	12.7	16.4	5.16	4.96
Co	3.85	0.87	3.1	1.24	0.14	4.78	2.25	0.5	0.11
Ni	73.6	44.4	65	27.5	1.82	63.3	29.6	6.63	1.42
Cu	6.16	2.48	3.59	1.52	0.21	1.59	1.26	0.28	0.06
Zn	15.6	10.1	580	634	6.74	10.2	29	14.4	15.8
Ga	0.21	0.05	0.45	0.15	0.02	0.61	0.89	0.03	0.02
Rb	1.09	0.22	3.35	0.5	0.13	4.08	6.16	0.25	0.06
Sr	13.7	72.8	202	25.1	4.69	289	101	4.88	2.55
Y	0.36	0.07	1.47	0.41	0.12	1.51	0.85	0.12	0.09
Mo	0.84	0.42	0.46	0.56	0.15	0.16	0.25	0.12	0.07
Cd	0.08	0.02	3.07	1	0.01	0.04	0.11	0.02	0.02
In	—	—	0.01	—	—	—	0.01	—	—
Sb	2.01	0.01	0.88	1.5	0.06	0.09	0.47	0.11	0.03
Cs	0.23	0.02	1.18	0.14	0.01	1.06	3	0.04	0.01
Ba	7.91	5.42	19.6	7.37	3.85	55.5	21.8	5.38	2.28
La	0.27	0.07	0.98	0.15	0.05	1.14	1.57	0.07	0.08
Ce	0.46	0.11	1.95	0.31	0.06	1.96	2.88	0.17	0.04
Pr	0.07	0.01	0.26	0.04	0.01	0.26	0.3	0.02	0.02
Nd	0.23	0.05	1.03	0.16	0.06	1.12	1.35	0.07	0.11
Sm	0.06	0.01	0.18	0.03	0.02	0.29	0.22	0.03	0.02
Eu	0.01	—	0.06	0.01	0.01	0.04	0.06	0.01	0.01
Gd	0.04	0.01	0.25	0.06	0.02	0.23	0.22	0.03	0.02
Tb	0.01	—	0.05	0.01	—	0.05	0.03	—	—
Dy	0.05	0.02	0.26	0.07	0.04	0.23	0.13	0.03	0.02
Ho	0.01	—	0.05	0.02	—	0.05	0.03	—	—
Er	0.04	0.01	0.14	0.05	0.01	0.12	0.08	0.03	—
Tm	0.01	—	0.02	0.01	—	0.02	0.01	—	—
Yb	0.06	0.01	0.14	0.05	0.01	0.12	0.1	0.02	0.01
Lu	0.01	—	0.02	0.01	—	0.02	0.02	—	—
W	0.35	0.55	0.46	0.31	0.19	0.86	0.49	0.48	0.21
Re	—	—	—	—	—	—	—	—	—
Tl	0.03	0.01	0.27	0.03	0.02	0.03	0.22	0.06	0.02
Pb	3.49	1.16	127	116	0.74	1.19	15	4.03	1.32

Table 2 (continued)

Element	BX-3 Magnesite	BX-4 Magnesite	BX-5A Dolomite	BX-5B Magnesite	BX-6 Magnesite	BX-8 Dolomite	BX-9 Dolomite	LMK-2 Magnesite	BX-12 Magnesite
Bi	–	–	0.03	0.01	–	0.03	0.03	–	–
Th	0.24	0.04	0.64	0.12	0.04	0.6	0.58	0.06	0.02
U	0.77	0.46	3.35	0.88	0.26	0.46	1.85	0.36	0.1
Nb	0.16	0.09	0.11	0.04	0.06	0.57	0.15	0.04	0.02
Ta	0.01	–	–	–	–	0.09	–	–	–
Zr	0.85	0.23	1.75	0.58	0.06	3.91	1.6	0.22	0.07
Hf	0.02	0.01	0.04	0.01	0.01	0.07	0.07	0.01	–
δEu	1.12	–	1.16	0.89	2.07	0.75	1.24	0.76	2.16
δCe	0.72	0.94	0.84	0.83	0.65	0.79	0.91	0.95	0.26
Eu/Sm	0.17	–	0.33	0.33	0.5	0.14	0.27	0.33	0.5
Sr/Ba	1.73	13.43	10.31	3.41	1.22	5.21	4.63	0.91	1.12

Table 3 Carbon and oxygen isotopic composition of magnesite and its surrounding rock

Sample	lithology	$\delta^{13}\text{C-V-PDB}$ (‰)	$\delta^{18}\text{O-V-PDB}$ (‰)	z
BX-3	Magnesite	8.4	−3.5	142.61
BX-4	Magnesite	8.2	−3.3	142.30
BX-5A	Dolomite	7.7	−9.8	138.06
BX-5B	Magnesite	8.1	−7.3	140.11
BX-6	Magnesite	8.3	−1.3	143.49
BX-8	Dolomite	5.9	−10.3	134.12
BX-9	Dolomite	6	−8.4	135.27
LMK-2	Magnesite	9.1	−3.9	143.84
BX-12	Magnesite	8.2	−2.6	142.64

Sr concentrations range between 101.0 and 289.0 ppm, which are significantly higher than those in magnesite samples.

4.2.2 Carbon–oxygen isotopes

In this study, carbon and oxygen isotope tests were performed on samples from the magnesite layer and surrounding rock dolomite to analyze their genesis. Table 3 presents the analysis and test values for the nine carbon and oxygen isotopes. Table 3 summarizes the ^{13}C values for magnesite samples with ore bodies ranging from 8.1‰ to 9.1‰, averaging at 8.38‰, while the $\delta^{18}\text{O}$ values range from −7.3‰ to −1.3‰, with an average value of −3.65‰. For the surrounding rock dolomite, the ^{13}C values range from 5.9‰ to 7.7‰, averaging 6.53‰, and the $\delta^{18}\text{O}$ values range from −10.3‰ to −8.3‰, averaging −9.5‰.

5 Discussion

5.1 Characteristics and petrographic evidence of non-hydrothermal metasomatic deposits

The magnesite and dolomite are uniformly distributed in the magnesite-bearing layer. Their presence aligns with the interlayer within the ore layer, maintaining a consistently stable horizon. The boundaries between these minerals and the surrounding rock, both above and below, are clear and strictly governed by the formation's distribution. The characteristics of the magnesite deposit in Baxia demonstrate the preservation of the original sedimentary features of the ore layer. Notably, the dolomite found in magnesite samples does not originate from hydrothermal metasomatic sources, as evidenced by the distinct boundary between them. In instances of hydrothermal fluid metasomatism, dolomite and magnesite displayed pronounced hydrothermal alteration and a gradual transition, as reported by Hu et al. (2022) and Huang and Zhang (2020). However, the ore deposit shows no significant alteration phenomena, and the texture of the ore remains uniform. The XRD analyses of whole rock samples reveal a high magnesite content in the ore-bearing layer. The primary minerals in the ore are exclusively magnesite and dolomite, with secondary minerals including quartz and trace amounts of pyrite. The simple and stable mineral composition, mirroring that of the surrounding rock, indicates a direct link between the deposit's formation and the surrounding rock dolomite. Microanalysis of thin sections shows that petrological characteristics of magnesite predominantly display a micritic texture alongside crust, block, breccia-like, and occasionally bedding structures. The irregular fissure columnar magnesite, filled with micritic magnesite and dolomite breccia, features a curved algal lamellar structure in larger grains, forming a crustal structure. Scholars studying the crust-grape-like structure of

dolomite in the Dengying Formation in the Sichuan Basin have suggested that such structures indicate deposition by biochemical processes in stable seawater environments (He et al. 2022; Mou et al. 2015; Qian et al. 2017). The magnesite in the study area displays micrite and crust-like structures, indicative of a sedimentary origin. Locally, algal lamellar deposition is notably present. Field characteristics and petrographic examinations lead to the inference that the genesis of magnesite is not directly linked to metasomatism by ultramafic, magnesia-rich fluids in the region.

5.2 Geochemical evidence supporting the origin of non-hydrothermal metasomatism

5.2.1 Elemental geochemistry

Liu et al. (2010) suggested that Fe-containing magnesite is closely associated with the origin of magnesium. The average geochemical iron content in ultramafic and mafic rocks is approximately 9%, whereas seawater represents a low Mn and Fe sedimentary environment, with significantly lower Mn and Fe contents than those found in freshwater. In general, magnesia from ultramafic rocks has a high iron content, reaching up to 5%, which is markedly higher than that in sedimentary environments ($\leq 1\%$) (Liu et al. 2010). Table 2 presents that the average Fe content in the magnesite-bearing layer is 0.15%, with two samples registering values below the detection limit. In contrast, the average Fe content in the surrounding dolomite rock is 0.46%. The relatively low Fe content in both magnesite and dolomite in Baxia implies the possible formation of these minerals in a sedimentary environment, showing no correlation with the weathering and leaching of ultramafic rocks.

Certain researchers have noted that a Sr/Ba ratio exceeding 1 indicates the formation of carbonates in marine depositional environments, whereas a ratio below 1 suggests their formation in continental settings (Huang 1997; Tao et al. 2009). In the Changdu area, dolomite in the magnesite deposit exhibits a high Sr content and a low Ba value, resulting in a Sr/Ba ratio above 1. Although the Sr and Ba contents in the magnesite of the ore-bearing layer are generally lower, their Sr/Ba ratio exceeds 1. These findings suggest a marine depositional environment for both the surrounding rock and the ore-bearing layer. The notable decrease in Sr content in the ore-bearing layer may be due to freshwater leaching. The Sr/Ba values in ultramafic rocks in the western part of Baxia range from 0.08 to 0.21, with an average of 0.13 (Yu et al. 2021). In this study, the Sr/Ba value in magnesite samples was found to vary between 0.90 and 13.43, with an average of 3.63, while that of the surrounding rock dolomite was in the range from 4.63 to 10.31, with an average of 6.72. Based on this trace element

data, the Sr/Ba ratio of magnesite samples is significantly higher than that of ultramafic rocks but lower than that of the surrounding rock dolomite. This observation indicates that the primary material for magnesite mineralization originates from magnesite carbonate formations and is not related to rocks of other origins.

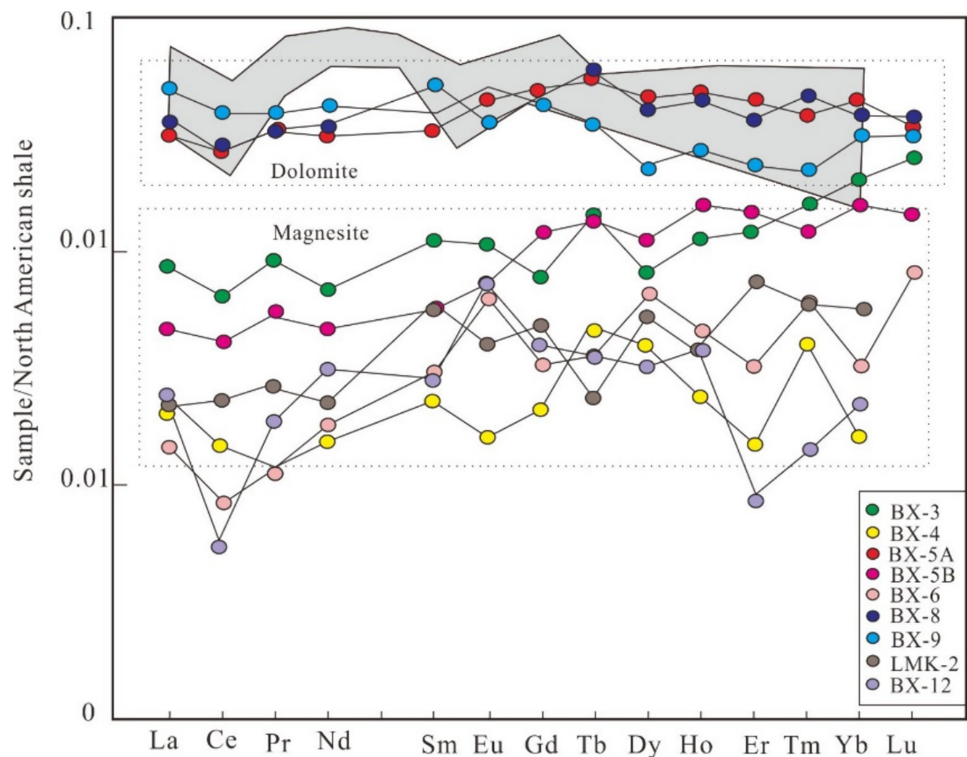
In carbonates, rare earth elements (REEs) generally do not migrate during diagenesis. Therefore, the geochemical characteristics of REEs are utilized to investigate the properties of carbonates and associated fluids during this process (Gong et al. 2021). This study compares the concentrations of REEs from the ore-bearing stratum and the surrounding magnesite rock with the average of the North American Shale Composite (Fig. 4). The findings indicate that the distribution pattern of REEs in dolomite is consistent with that in carbonates from various global regions. This consistency suggests that the dolomite in this area may have formed through evaporation deposition in the basin. Notably, the distribution pattern of magnesite significantly diverges from that of the surrounding dolomite. Both minerals exhibit a similar flat pattern for REEs. The negative δCe anomalies in both dolomite and magnesite from the surrounding rock indicate their formation in a reducing environment.

The Eu/Sm ratio in samples ranges from 0.14 to 0.50, with an average of 0.32, aligning with sedimentary rock values (Pan 2015). Both magnesite and dolomite show slight depletion in Ce and enrichment in Eu. Typically, dolomite evaporation under oxic conditions results in Eu enrichment and Ce depletion. This phenomenon may be related to increased water salinity from enhanced evaporation in the depositional environment, thereby raising the ratio of $\text{Mg}^{2+}/\text{Ga}^{2+}$. Studies suggest that dolomite formed from mixed water typically lies in the transitional zone between freshwater and seawater undercurrents, leading to less pronounced differentiation in Ce (Li and Yang 2005). Considering these Ce characteristics, the magnesite and dolomite strata likely deposited in an environment with reduction–oxidation conditions, displaying mixed water doping characteristics. The REEs partition curves of the studied dolomites are consistent with global averages for carbonates. The formation of magnesite may be attributed to basin evaporation and concentration, where Mg^{2+} -rich brine replaces Ca^{2+} in dolomite, forming magnesite.

5.2.2 Isotopic geochemistry

The $\delta^{13}\text{C}$ (PDB) in modern seawater varies from $-2\text{\textperthousand}$ to 2\textperthousand , while in freshwater, it ranges from $-5\text{\textperthousand}$ to $-11\text{\textperthousand}$. Carbonates associated with marine facies typically range from $-5\text{\textperthousand}$ to $+5\text{\textperthousand}$ (Wei et al. 1988). From the Cambrian to the Pliocene, the average $\delta^{13}\text{C}$ value in marine limestone strata remains relatively stable at $0.56\text{\textperthousand} \pm 1.55\text{\textperthousand}$ (Keith and Weber 1964). For example, late Precambrian carbonates

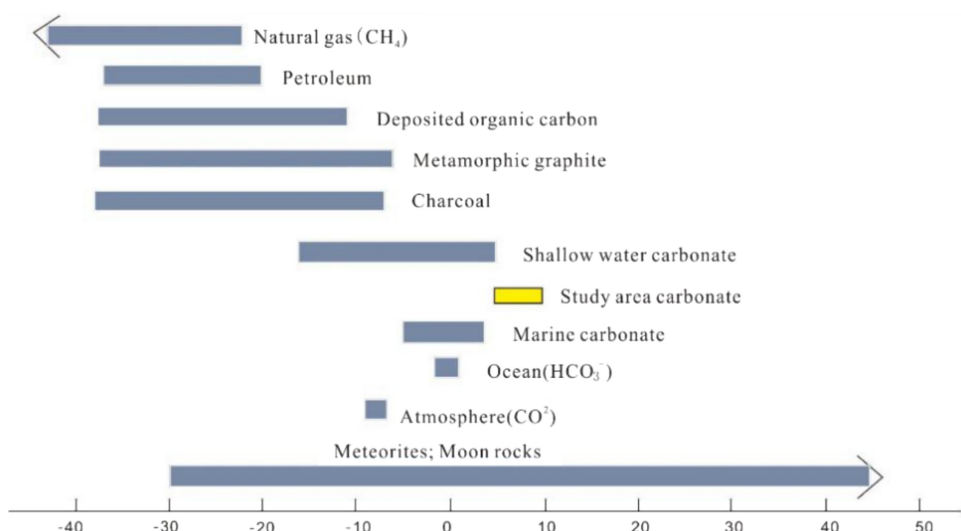
Fig. 4 Magnesite–dolomite samples standardized with North American shale (Taylor and McLennan 1985). Note: The gray area is the average range of carbonates deposited in different parts of the world (Luo 1990)



in Africa have $\delta^{13}\text{C}$ values similar to those for the Phanerozoic (Schidlowski et al. 1975). Late Paleozoic to Cenozoic marine carbonates generally hover around 0‰, varying between 3‰ and 5‰ (Zhang 1985). In the study area, carbonate rock $\delta^{13}\text{C}$ ranges from 5.9‰ to 9.1‰, which is markedly higher than the typical sedimentary range for marine carbonates (Fig. 5) and exceeds the average $\delta^{13}\text{C}$ range from the Cambrian to the Paleogene. Furthermore, the $\delta^{13}\text{C}$ distribution of the samples in this study notably surpasses those of both marine and shallow water carbonates. The

accumulation of $\delta^{13}\text{C}$ in carbonates can occur moderately in environments with seawater evaporation or high salinity (Wang 1994). Therefore, the elevated $\delta^{13}\text{C}$ values in this area may be due to seawater evaporation and concentration. Frank and Fielding (2003) posited that the Mg-containing fluid forming magnesite primarily originated from plutonic and supergene fluids or a combination thereof, leading to distinct geochemical characteristics in magnesite precipitated from these fluids. The magnesite in ultramafic rocks usually shows a marked $\delta^{13}\text{C}$ deficit (−5‰ to −20‰), while that

Fig. 5 Isotopic composition of carbon in natural materials and lithotypes (Wei and Wang 1988)



in magnesium-rich carbonate strata typically displays high $\delta^{13}\text{C}$ values (2.3‰–8‰) (Kralik et al. 1989; Schroll 2002). Table 3 presents that the $\delta^{13}\text{C}$ values of the magnesite-bearing layer range from 8.1‰ to 9.1‰, substantially higher than those from metasomatic mineralization. It suggests that the hypothesis of magnesite's metallogenetic material originating from ultramafic rocks or fluid weathering leaching is implausible. Instead, magnesium-rich carbonates are more likely the source, providing ample magnesium for deposit formation.

The $\delta^{18}\text{O}$ values of magnesite samples in the study area range from –7.3‰ to –1.3‰, whereas those of the surrounding dolomite rocks range from –10.3‰ to –8.4‰. This difference indicates that the $\delta^{18}\text{O}$ values of magnesite are notably higher than those of dolomite. Furthermore, the oxygen isotope projection maps for various geological reservoirs (Fig. 6) demonstrate that certain samples in this study align with the range of seawater values, exhibiting an overall range markedly higher than those of seawater and other rocks. The oxygen isotope composition also suggests the impact of terrestrial water or atmospheric precipitation in the study area. From the perspective of seawater evaporation and concentration, the transition from dolomite to magnesite shows signs of declining salinity and the inclusion of terrestrial water or atmospheric precipitation. Given the influence of temperature on $\delta^{18}\text{O}$ values, the transition indicates a decrease in temperature (Hudson 1977; Shackleton and Kennett 1976). If metasomatism of magnesium-rich ultramafic fluid had occurred in the region, its temperature trend might have contrasted with the observed decrease, contradicting the findings of this study. Based on the oxygen isotope values of magnesite and dolomite, the formation process from dolomite to magnesite during seawater evaporation corresponds to the interpretations derived from the test data.

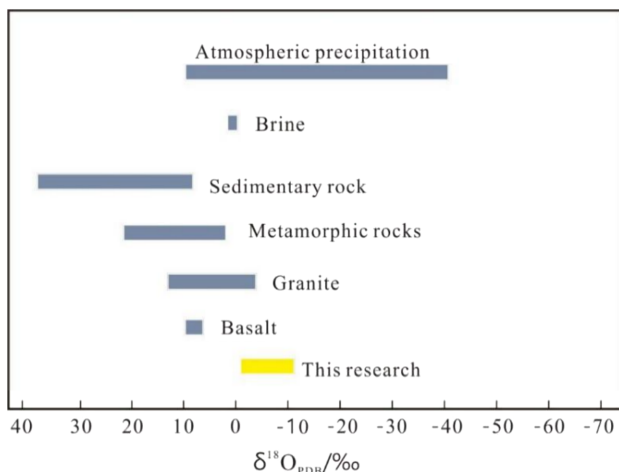


Fig. 6 $\delta^{18}\text{O}$ values in different geological environments (Hoefs 1980)

Continental carbonates typically accumulate in freshwater environments with lower $\delta^{18}\text{O}$ values, benefiting from a greater influx of organic matter in sedimentary basins compared to that in oceanic basins. Consequently, the $\delta^{18}\text{O}$ and $\delta^{13}\text{C}$ values of continental carbonates usually fall below those of marine carbonates. Keith and Weber (1964) proposed an empirical formula for determining the sedimentary environment of carbonates since the Jurassic:

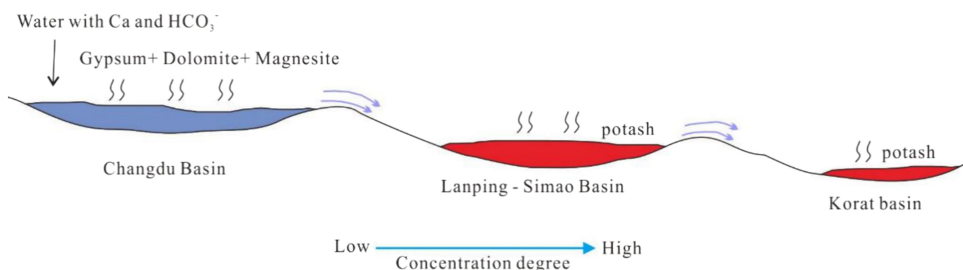
$$Z = 2.048 \times (\delta^{13}\text{C} + 50) + 0.498 \times (\delta^{18}\text{O} + 50)$$

where $\delta^{18}\text{O}$ and $\delta^{13}\text{C}$ are based on the PDB. The Z value exceeding 120 indicates a marine depositional environment, while Z value below 120 suggests a continental depositional environment. The absolute Z value also provides insights into the relative salinity of the sedimentary water. However, noteworthy, Z values above 120 can occur for carbonates that formed in terrestrial environments with significant evaporation. In this study, the Z values of nine magnesite samples from Baxia were calculated. All samples yielded Z values above 120 (Table 3), suggesting that the carbonates of magnesite likely originated in a marine depositional environment with high salinity.

5.3 Indicative significance of magnesite in the regional potash-forming process

The perspective that the evaporites in the Lanping–Simao–Korat Basin are of Marine origin and continental origin has been supported by many scholars (Miao et al. 2017; Tabakh 1999; Tan et al. 2010; Gao et al. 2013; Wang et al. 2014a, b). Lithofacies paleogeography indicates that during the Late Cretaceous, the Changdu–Simao–Korat Block exhibited an almost east–west orientation, characterized by widespread shallow sea and coastal deposits in the Qiangtang Basin, particularly in the Changdu area (Li et al. 2001). This region is distinguished by its abundant Jurassic and Cretaceous gypsum deposits and magnesite, with properties indicative of sedimentary genesis, and serves as a prominent example in the Changdu Basin. The salt strata in the Changdu–Lanping–Simao–Korat Basin have very similar provenance regions, and they correspond to pan-basin systems with interconnected provenance during the transgression stage, indicating that there is a certain provenance connection between these basins in the pre-salting period (Wang et al. 2014a, b; Han et al. 2021). From the perspective of regional metallogenetic geological characteristics, only a small amount of sulfate rock and carbonate rock exist in the potassium salt mines in Lanping–Simao and Korat Basins, and the ratio of sulfate rock and carbonate rock is far from consistent with the normal sequence of seawater evaporation and deposition.

Fig. 7 Migration direction of metamorphic seawater between the Basins



However, numerous contemporaneous Marine sulfate and carbonates have developed in the Changdu Basin and the Qiangtang Basin. The distribution characteristics of carbonate rock minerals indicate that brine tends to gradually concentrate from Lanping–Simao Basin to Korat Basin (Qu 1998). Research on various geochemical indicators of salt spring water shows that the solute sources of exposed salt spring water in the Changdu Basin and the Lanping–Simao Basin are consistent, and show a trend of increasing gradually from the Changdu Basin to the Lanping–Simao Basin (Qin et al. 2017; Zhang et al. 2011). The results of seawater evaporation experiments reveal that magnesite can only be formed when continental water containing Ca^{2+} and HCO_3^- is added to the water body (Li 2015). Magnesite does not precipitate in seawater under normal evaporation conditions (Chen 1983; Li and Han 1995). Therefore, magnesite indicating the presence of brine water in the Mengyejing deposit may have transformed continental water bodies. This study further confirms that the carbonates in the Changdu Basin may be of sedimentary origin, and the source of magnesium may be seawater.

All the above-mentioned evidences indicate the presence of a close relationship between the potash-forming process in the Changdu–Lanping–Simao Basin. Therefore, the salt and potash formation patterns in the East Tethys salt-bearing basins exhibit distinct characteristics. The Nujiang Tethys concluded its evolutionary course in the Late Cretaceous, while the Nujiang area continued to undergo collision and orogeny. Influenced by these tectonic activities, residual metamorphic seawater in the Changdu Basin possibly migrated to the Lanping–Simao Basin and even Korat Basin, leading to the extensive deposition of potash in these regions. The early stages of potash sediment formation in the Changdu Basin involved the deposition of marine sulfate rocks and carbonates. These observations indicate that the Changdu Basin displays the characteristics of an initial basin within the broader regional context of salt and potash formation (Fig. 7).

6 Conclusions

Based on petrographic observations and geochemical analyses of magnesite and dolomite samples obtained from the magnesite deposit in Baxia, Changdu Basin, the following conclusions were drawn:

1. Magnesite exhibits a stratified structure, with a well-defined boundary between the magnesite-bearing layer and the surrounding dolomite rock. The mineralogical composition is relatively simple, consisting primarily of magnesite and dolomite, along with secondary minerals such as quartz and trace amounts of pyrite. Petrographic examinations reveal crustal and algal lamellar structures suggestive of sedimentary origin. Both field observations and petrographic studies confirm that the deposit is of sedimentary origin.
2. Elemental and isotopic geochemistry analyses of magnesite and dolomite samples from the magnesite deposit indicate their formation in a high-salinity environment. The genesis of magnesite may involve the replacement of magnesium ions for calcium ions in previously formed dolomite during evaporation, concentration, and sedimentation processes. Magnesite and dolomite exhibit a genetic relationship, with the magnesia source being closely linked to seawater, as opposed to magnesia-rich fluid replacing dolomite in ultramafic rocks within the region.
3. Based on the integration of the findings of this study with existing data, the regional salt and potash-forming model is further corroborated. This model suggests that water bodies with high concentrations of residual metamorphic deposits in the Changdu Basin migrated to the Lan-Ping Simao Basin and potentially extended to the Khorat Basin through the northern Laos and Nakhon Tai basins. This migration led to the deposition of numerous potash salt beds in these stable craton basins.

Acknowledgements The authors greatly acknowledge the financial support from the Second Tibetan Plateau Scientific Expedition and Research (Grant No. 2019QZKK0805), the postdoctoral project of

Qinghai Institute of Salt Lakes (Grant No. E260DZ0401), the Kunlun Talent Project in Qinghai Province (Grant No. E340DZ0801), and the Qinghai Provincial Department of Science and Technology Project (Grant No. 2024-ZJ-722). We are also thankful to the editors and anonymous reviewers for their valuable comments, which have helped to improve the quality of the final manuscript.

Author contributions Conceptualization: Wenhua Han and Yongshou Li; Methodology: Wenhua Han; Software: Wenhua Han; Validation: Yongshou Li and Haizhou Ma; Formal analysis: Wenhua Han and Yongshou Li; Investigation: Wenhua Han, Yongshou Li, Haizhou Ma, Huaide Cheng, Binkai Li, Xuahai Ma and Qinyu Hai; Resources: Yongshou Li; Data curation: Yongshou Li; Writing—original draft preparation: Wenhua Han; Writing—review and editing: Yongshou Li, Haizhou Ma, Huaide Cheng, Binkai Li, Xuahai Ma and Qinyu Hai; Supervision: Yongshou Li; Project administration: Yongshou Li; Funding acquisition: Haizhou Ma. All authors have read and agreed to the published version of the manuscript.

Declarations

Conflict of interest The authors declare that they have no conflict of interest.

References

- Chen YH (1983) Salt evolution sequence of Yellow Sea water at 25° constant temperature and distribution of some trace elements. *Acta Geologica Sin.* 04:379–390.
- Ding JH, Chen ZH, Yang GJ, Deng F, Lou DB (2013) Metallogeny and resource potential of magnesite deposits in China. *Geology in China.* 40(06):1699–1711.
- Frank TD, Fielding CR (2003) Marine origin for Precambrian, carbonate-hosted magnesite? *Geology.* 31(12):1101–1104.
- Gao X, Fang QF, Yao W, Peng Q, Dong J, Qin H, Di YW (2013) Genesis of the Mengyejing potash deposit in Lanping-Simao basin, Yunnan: Indication from the components of the deposit. *Acta Geosci Sin.* 34:529–536.
- Gong QL, Li F, Lu CJ, Wang HZ, Tang H (2021) Tracing seawater- and terrestrial-sourced REE signatures in detritally contaminated, diagenetically altered carbonates. *Chem Geol.* 570:120–169.
- Han WH, Ma HZ, Fang WX, Cheng HD, Li YS et al (2021) U-Pb Detrital Zircon ages and geochemical features of the Jingxing formation, (Qamdo Basin, Tibet: Implications): Inferences for the metallogenic model of the East Tethys Evaporite. *Minerals.* 11:745.
- He Y, Zhou JG, Chen X et al (2022) Genesis and geological significance of upper Sinian Dengying dolostone with grape-lace shaped cement Sichuan Basin. *Marine Orig Pet Geol.* 20(04):57–64.
- Hoefs J (1980) Stable isotope geochemistry. Springer Verlag, Berlin, p 208.
- Hu GY, Sun XS, Zheng J et al (2022) The genesis of Haicheng-Dashiqiao magnesite deposits, Liaodong Peninsula. *Acta Geol Sin.* 96:1340–1355.
- Huang SJ (1997) A study on carbon and strontium isotopes of Late Paleozoic Marine carbonates in the Upper Yangtze Platform. *Acta Geol Sin.* 01:45–53.
- Huang H, Zhang LC (2020) Genesis of the Lilaozhuang iron-magnesite deposit in the Huoqu area of Anhui Province: Indicative significance of Carbon and Oxygen isotopes. *Bull Mineral Petrol Geochem.* 39:072.
- Hudson DJ (1977) Stable isotopes and limestone lithification. *J Geol Soc London.* 133(6):637–660.
- Keith ML, Weber JN (1964) Isotopic composition and environmental classification of selected limestone and fossils. *Geochim Cosmochim Acta.* 28:1786–1816.
- Kralik M, Aharon P, Schroll E, Zachmann D (1989) Carbon and oxygen isotope systematics of magnesites: A review. *Monogr Ser Mineral Depos.* 28:197–223.
- Li YW, Han WT (1995) Experimental study on isothermal evaporation of seawater at 25°C in South China Sea. *Sci Geol Sin.* 30(03):233–239.
- Li ZH, Yang YH (2005) Present situation and progress of genetic research of dolomite. *Pet Geol Recover Effic.* 02:5–8.
- Li XH, Wang CS, Yi HS, Li Y (2001) Middle Cretaceous and Eocene lithofacies and paleogeography in Tibet. *Reg Geol China.* 20:82–88.
- Li YL, Wang CS, Li TN (2008) Characteristics of the Jurassic saline deposits and its significance to hydrocarbon accumulation in Qiangtang basin of Tibet area. *Acta Petrolei Sinica.* 29(02):17–178.
- Li YS (2015) Metallogenetic Model of the Cretaceous Potash-Bearing Evaporites Involving Changdu, Lanping-Simao and Khorat Basin. Dissertation, University of Chinese Academy of Sciences.
- Liang Q, Jing H, Gregoire DC (2000) Determination of trace elements in granites by inductively coupled plasma mass spectrometry. *Talanta.* 51:507–513.
- Liu LH, Huang SJ, Wang CL, Huang KK, Tong HP, Zhong QQ (2010) Cathodoluminescence zonal texture of calcite cement in carbonate rock and its relationship with trace element composition: A case of Ordovician carbonate rock of Tahe Oilfield Tarim Basin. *Mar Orig Pet Geol.* 15(01):55–60.
- Luo YX (1990) Activities and material sources of rare earth elements during magnesite mineralization in Dashiqiao. *Geol Rev.* 01:31–41.
- Miao ZY, Zhang Z, Zheng MP et al (2017) Tectonic Evolution of Eastern Tethys and Formation of Evaporite in Lanping-Simao, Basin Southwest China. *Acta Geosci Sin.* 38(6):883–896.
- Mou CL, Wang XP, Liang W, Liang W, Wang YC, Men X (2015) Characteristics and genesis of grape-like stone of dolomite in Sinian Dengying Formation in Yangtze region: a case from the first section of Dengying Formation in Yangba, Nanjiang Sichuan Province. *Acta Sedimentol Sin.* 33(06):1097–1111.
- Pan (2015) Discussion on genesis of magnesite deposit in Haicheng, Liaoning Province. *Sci Technol Commun.* 7(20):77–89.
- Pan GT, Wang LQ, Li RS (2012) Tectonic model of archipelagic arc-basin systems: The key to the continental geology. *Sediment Geol Tethyan Geol.* 32:1–20.
- Qi ZL (2017) Characteristics of the source rocks in Nangqian-Qamdo Area, Eastern Tibet: Implications for unconventional oil and gas resources, China University of Geosciences (Beijing).
- Qian YX, Feng JF, He ZL, Hang KY, Jin T, Dong SF, You DH, Zhang YD (2017) Applications of petrography and isotope analysis of micro-drill samples to the study of genesis of grape-like dolomite of the Dengying Formation in the Sichuan Basin. *Oil Gas Geol.* 38(04):665–676.
- Qin XW, Ma HZ, Zhang XY, Fan QS, Cheng DH, Li YS, Miao WL, Hai QY, Shi HY (2017) Hydrochemical characteristics of salt spring and potassium-prospecting in Changdu Basin. *J Salt Lake Res.* 25(02):28–39 (in Chinese with English abstract).
- Qu YH (1998) Metallogenetic regularity and prediction of potash salt in Laping-Simao Basin. Geology Press, Beijing, pp 61–65.
- Schidlowski M, Eichmann R, Junge CE (1975) Precambrian sedimentary carbonates: Carbon and oxygen isotope geochemistry and implications for the terrestrial oxygen budget. *Precambr Res.* 2(1):1–69.
- Schroll E (2002) Genesis of magnesite deposits in the view of isotope geochemistry. *Boletim Paranaense De Geociencias.* 50(50):59–68.

- Shackleton NJ, Kennett JP (1976) Paleotemperature history of the Cenozoic and the initiation of Antarctic glaciation; Oxygen and carbon isotope analyses in DSDP sites 277, 279 and 281. Initial Reports of the DSDP. 29.
- Su TN, Zhang WZ, Zhang SQ, Zhang H (2007) Geologic features of gypsum strata in the middle part of Buqu Formation, Biluocuo area. *Tibet Jilin Geol.* 26(02):10–15.
- Tao SH, Tang DZ, Zhou CW, Li F, Li JJ, Chen XZ, Meng CA (2009) Element geochemical characteristics of the lower assemblage hydrocarbon source rocks in southeast Sichuan-central Guizhou (Chuandongnan-Qianzhong) region and its periphery areas and their implications to sedimentary environments. *Geol China.* 36(02):397–403.
- Taylor SR, McLennan SM (1985) The continental crust: Its composition and evolution. *J Geol.* 94(4):57–72.
- Wang KF (1994) Carbon isotopic composition of Marine carbonate and its significance. *Sci J Earth Sci.* 05:50–54.
- Wang LC, Liu CL, Fei MM, Shen LJ, Zhang H (2014a) Sulfur isotopic composition of sulfate and its geological significance of the Yunlong formation in the Lanping Basin, Yunnan Province. *China Min Mag.* 23:57–63.
- Wang LC, Liu CL, Gao X, Zhang H (2014b) Provenance and paleogeography of the Late Cretaceous Mengyejing Formation, Simao Basin, southeastern Tibetan Plateau: Whole-rock geochemistry, U-Pb geochronology, and Hf isotopic constraints. *Sediment Geol.* 304:44–58.
- Wei JY, Wang GY (1988) Isotope geochemistry. Geology Publishing House.
- Wu FY, Wan B, Zhao L, Xiao WJ, Zhu RX (2020) Tethyan geodynamics. *Acta Petrol Sin.* 36(03):1627–1674.
- Xie XW (2007) Report of regional geological survey: Nangqian County, Changdu County, Jiangda County; Tibet Institute of Geological Survey: Tibet, China, pp 107–109.
- Yu T, Zhou X, Fan BL, SH N, He JJ, Yu JS, Yi JL, (2021) Petrogeochemical and Pb-Nd-Sr isotope characteristics of ultramafic rocks in the Yizhuxingla area, Eastern Tibet. *Geol Bull China.* 40(5):687–697.
- Zhang XL (1985) Relationship between stable isotopes of oxygen and carbon in carbonates and paleo-salinity and paleo-water temperature. *Acta Sedimentol Sin.* 04:17–30.
- Zhang CW, Gao DL, Zhang XY, Tang QL, Shi L (2011) Comparison of geochemistry characteristics in Palaeocene salt-bearing Strata of Lanping-Simao Basin and Chuxiong Basin. *J Salt Lake Res* 19(03):08–14 (in Chinese with English abstract).

Springer Nature or its licensor (e.g. a society or other partner) holds exclusive rights to this article under a publishing agreement with the author(s) or other rightsholder(s); author self-archiving of the accepted manuscript version of this article is solely governed by the terms of such publishing agreement and applicable law.